THE SCATTER FOCUSSING OF MULTI-GeV
CHARGED PARTICLES AND NEUTRAL HADRONS*

LAWRENCE W. JONES and DONALD G. KOCH

Randall Laboratory of Physics, University of Michigan, Ann Arbor, Michigan 48104, U.S.A.

The multiple Coulomb scattering of charged particles and the nuclear elastic scattering of neutral hadrons may serve as a basis for the design of lenses for beams of such particles. The optical and spectral properties of such lenses are explored and numerical examples are given.

1. Introduction

Charged particles may be focussed by multiple scattering in a suitably designed lens of scattering material. Similarly, neutral hadrons may be focussed by elastic scattering from nuclei using a specially constructed lens.

These notions and some experimental observations were originally set forth in papers by one of us in 1964 on *The random optics of particle beams*[1]. In this paper, we present a more complete – and more correct – formulation of the multiple-scattering focussing problem, with numerical examples. We then present a quantitative study of the elastic scattering lens for neutrons (or other neutral hadrons) noting possible applications and numerical examples.

The history of this interest began in 1963 when setting up experiments in the extracted proton beam of the Brookhaven Cosmotron. Polaroid film constituted a convenient detector technique for aligning and focussing the beam. In order to locate a reference point or line on the film, a metal object was placed at a known position ahead of the film and its shadow was recorded on film. The curious properties of these shadows, or (more properly) images, was the starting point for the ideas discussed below. If the film is placed against an object, no image is seen, but if the film is a few cm beyond the object, the image is surprisingly sharp and detailed. That no image is seen in the former case in reasonable, since the attenuation of a 3 GeV proton beam in $\frac{1}{8}''$ of brass is only about 2%. The image that develops with spacing is then due to multiple Coulomb scattering in the metal.

In order to understand such images, consider a Cartesian coordinate system with a parallel beam in the $+z$ direction and a scattering slab at $z = 0$ extending over all y and all positive x ($x \geq 0$) with open space

at all negative x. Neglecting interactions in the slab, the beam flux at $x \gg 0$ and at $x \ll 0$ for positive values of z is unaffected by the slab, since as much flux is scattered into a given area as out of one. On the other hand, for values of x near $|x|/z \approx \theta_{rms}$ (where θ_{rms} is the multiple Coulomb scattering angle), the intensity will be reduced for x positive, since some particles are scattered out of that region, and the intensity will be
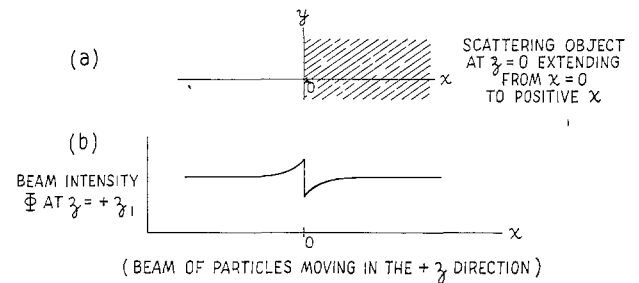

Fig. 1 The nature of an image resulting from a semi-infinite slab of scattering material. (a) The scatterer, at $z = 0$; (b) the particle flux Φ vs x at $z_1 > 0$.
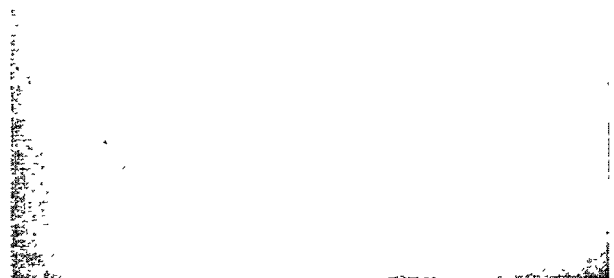

Fig. 2. Scatter images of cylinders of lead (left) and aluminum (right) in a proton beam of 3 GeV. Each cylinder was 1″ in diameter and 1″ in length. The film was 15″ beyond the cylinders. The images are positive prints, i.e., lighter shades are higher intensity.

increased for x negative since no particles are scattered out but some are scattered in. This is illustrated in fig. 1. In fig. 2 we have reproduced the image of two $1''$ diameter, $1''$ long cylinders (axes parallel to the proton beam), one of lead and one of aluminum. The images are positive prints, so that bright areas correspond to higher proton fluxes. That more subtle image detail may be visualized is seen in figs. 3 and 4, where a wrist watch and an electric hand drill are imaged.

2. A multiple Coulomb scattering lens

The notion that multiple Coulomb scattering can be used to enhance the flux of charged-particle beam particles at some region downstream of a scatterer suggests that it should be possible to so arrange
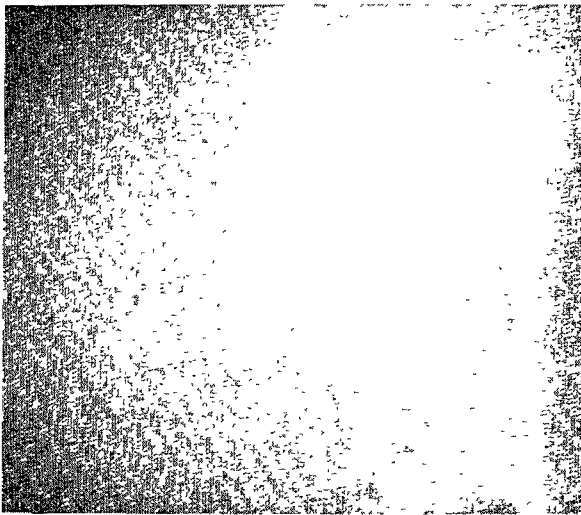

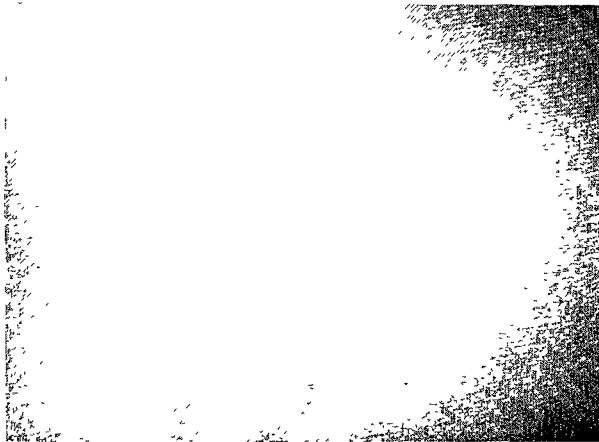Fig. 3. A wrist watch imaged by scattering of 3 GeV protons.

Fig. 4. A portion of an electric hand drill imaged with 3 GeV protons.

scatterers as to maximize this flux enhancement, i.e., to design a "lens". We may proceed below with such a lens design, making use of simplified expressions for multiple Coulomb scattering[2].

The probability of scattering through a projected angle θ_x upon traversal of a scattering material of thickness l is given by

$$P(\theta_x)\mathrm{d}\theta_x = \frac{1}{\theta_0}\left(\frac{2}{\pi}\right)^{\frac{1}{2}}\exp-[\theta_x^2/2\theta_0^2]\,\mathrm{d}\theta_x, \tag{1}$$

where

$$\theta_0 = \frac{15.0}{pv}(l/l_\mathrm{R})^{\frac{1}{2}} = (\theta_x)_\mathrm{rms}, \tag{2}$$

with pv in MeV and l_R the radiation length in the material. The probability of scattering through a space angle θ is then

$$P(\theta)\mathrm{d}\theta = \frac{\theta}{\theta_0^2}\exp-[\theta^2/2\theta_0^2]\,\mathrm{d}\theta, \tag{3}$$

where

$$(\theta)_\mathrm{rms} = \sqrt{2}(\theta_x)_\mathrm{rms} = \frac{21.2}{pv}(l/l_\mathrm{R})^{\frac{1}{2}}. \tag{4}$$

In these expressions and throughout we will use only the small angle approximation where $\theta \cong \sin\theta \cong \tan\theta$. The probability of scattering into a solid angle $\mathrm{d}\Omega$ at θ is then

$$\frac{P(\theta)}{2\pi\theta}\,\theta\,\mathrm{d}\theta\,\mathrm{d}\varphi = \frac{P(\theta)}{2\pi\theta}\,\mathrm{d}\Omega. \tag{5}$$

Now consider a uniform parallel flux Φ_0 of particles (of p, v) incident on a scattering slab of thickness l at $z = 0$ as in fig. 5. At r from the z axis the number of particles incident on a small area $\mathrm{d}A_0$ will contribute to the flux at $z = d$, $r = 0$ an amount $\mathrm{d}\Phi$ given by

$$\mathrm{d}\Phi = \Phi_0\,\mathrm{d}A_0\left[\frac{P(\theta)}{2\pi\theta}\right]\frac{\mathrm{d}\Omega}{\mathrm{d}A_d}, \tag{6}$$
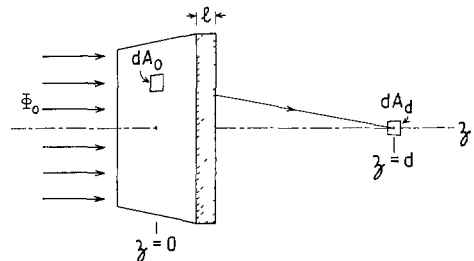

Fig. 5. Scattering of a parallel beam by a plane slab of thickness l.

where dA_d is an element of area normal to the z axis at $z = d$. Then, in the small angle approximation,

$$d\Omega \cong dA_d/d^2,$$

$$r/d \cong \theta,$$

and

$$dA_0 = r\,dr\,d\varphi.$$

Therefore,

$$d\Phi = \Phi_0 \frac{d\varphi}{2\pi} P(\theta)d\theta. \qquad (7)$$

Integrating around an annulus of radius r and width dr over φ from 0 to 2π gives

$$d\Phi = \Phi_0 P(\theta)d\theta. \qquad (8)$$

If we now use a scatterer in the shape of a disc of inner radius r_1 and outer radius r_2, subtending angles from the "focal" plane ($z = d$, $r \cong 0$) $\theta_1 \cong r_1/d$, $\theta_2 \cong r_2/d$, the total flux Φ_T in this focal plane is given by

$$\Phi_T = \Phi_0\left[1 + \int_{\theta_1}^{\theta_2} P(\theta)d\theta\right] > \Phi_0, \qquad (9)$$

so that some net gain in flux is achieved.

One can do better than use a uniform slab, of course. The scatterer may be contoured in the form of a paraboloid of revolution such that

$$\theta = \alpha\theta_0,$$

or

$$\frac{r}{d} = \frac{15\alpha}{p\upsilon}(l/l_R)^{\frac{1}{2}}, \qquad (10)$$

so that $l \propto r^2$.

Now

$$\Phi_T = \Phi\left[1 + \int_{\theta_1}^{\theta_2} \frac{\alpha^2}{\theta} \exp(-\tfrac{1}{2}\alpha^2)d\theta_0\right], \qquad (11)$$

or

$$\Phi_T = \Phi\left[1 + \alpha^2 \exp(-\tfrac{1}{2}\alpha^2)\ln(\theta_2/\theta_1)\right]. \qquad (12)$$

For fixed θ_1 and θ_2, Φ_T is maximum for $\alpha = \sqrt{2}$, or

$$\Phi_T/\Phi_0 = \left[1 + \frac{2}{e}\ln(\theta_2/\theta_1)\right] \qquad (13)$$

$$\Phi_T/\Phi_0 = [1 + 0.7358\ln(\theta_2/\theta_1)].$$

This geometry is illustrated in fig. 6.

The spectral properties of the lens, or chromatic aberration, can be found by study of eq. (8), which we may rewrite here as

$$d\Phi(p) = \Phi_0(p)\frac{\theta\,d\theta}{\theta_p^2}\exp-[\theta^2/2\theta_p^2], \qquad (14)$$

where θ_p is the r.m.s. scattering angle for particles of momentum p and $\Phi(p)$ is the flux of those particles. From eq. (2),

$$p\theta_p = p_0\theta_0,$$

and from eqs. (12) and (13),

$$\theta = \theta_0\sqrt{2},$$

so that

$$\theta_p = \frac{p_0\theta}{p\sqrt{2}}. \qquad (15)$$

Consequently

$$d\Phi(p) = \Phi_0(p)2\left(\frac{p}{p_0}\right)^2 \exp-[p^2/p_0^2]\frac{d\theta}{\theta}, \qquad (16)$$

and

$$\Phi(p) = \Phi_0(p)\,2\left(\frac{p}{p_0}\right)^2 \exp-[p^2/p_0^2]\ln\left(\frac{\theta_2}{\theta_1}\right). \qquad (17)$$

The ratio of the flux at p relative to the flux at p_0, the design momentum, can then be found relative to the incident flux at each momentum. This is:

$$\frac{\Phi(p)/\Phi_0(p)}{\Phi(p_0)/\Phi_0(p_0)} = \left(\frac{p}{p_0}\right)^2 \exp[1 - (p^2/p_0^2)]. \qquad (18)$$

As before, $\Phi_T = \Phi + \Phi_0$, however it is convenient to leave eq. (18) in this form as it is independent of θ_2/θ_1. The response function of eq. (18) is plotted in fig. 7.

Consider a numerical example of such a scatter focussing lens where $\theta_2/\theta_1 = 20$. Here, for the design
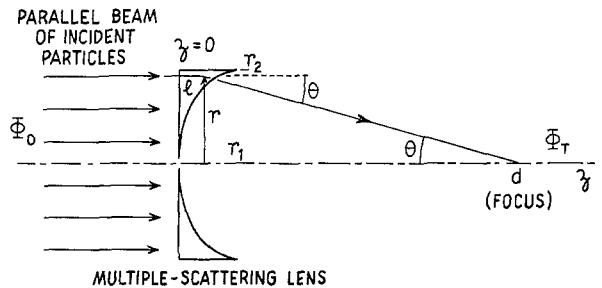

Fig. 6. The geometry of a multiple scattering lens, with a thickness $l \propto r^2$ from r_1 to r_2.

momentum p,

$$\Phi_T/\Phi_0 = 3.204. \tag{19}$$

This might in practice correspond to a lens of 20 cm outer diameter with a 1 cm diameter hole in the center. This could be a lead lens of 20 cm diameter and 1/5 of a nuclear interaction mean free path thick at the edge. Since the interaction mean free path in lead is about 14 cm, it would be 2.8 cm thick at $r = 10$ cm. As $l_R = 0.51$ cm for lead, the focal length would then be found from

$$r/f = r/d = \theta_2 = \frac{15}{pv}\sqrt{(2.8/0.51)} = \frac{35.147}{pv} \tag{20}$$

The focal length is then given by

$$f = \frac{pv\, r_2}{15.0}\,(l_R/l_2)^{\frac{1}{2}}, \tag{21}$$

which, for this numerical example, gives

$$f = 0.2845(pv).$$

where pv is in MeV and f is in cm. Thus for $pv = 10\,\mathrm{GeV}$ $f = 28.45$ m.

This lens would enhance the axial flux over the central 1 cm diameter spot by a factor of 3.2, and with a focal length altogether reasonable. Such a lens is obviously very much less costly than a magnetic lens (quadrupole pair, etc.), it is compact and trouble-free. As such it could be totally buried in shielding, or could be used in an intense radiation environment. On the other hand, the gain through scatter focussing should not be misunderstood. Our factor of 3.2 should properly be compared with a factor of 400 for a properly designed magnetic lens of the same aperture.
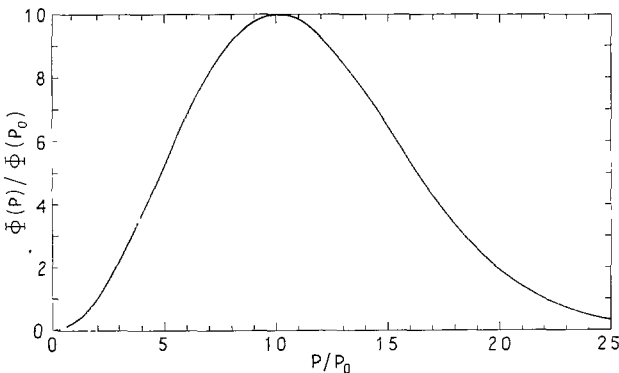
In fact the gains in scatter focussing are proportional to ln (aperture) while the gains in proper geometrical optics are proportional to (aperture)^2.

3. Elastic scatter focussing of neutral hadrons

3.1. GENERAL PRINCIPLES

The situation is somewhat more interesting in the case of neutral hadrons where no other focussing is possible. Here nuclear diffraction elastic scattering plays a role exactly analogous to multiple Coulomb scattering (section 2) except that atomic mass number (nuclear radius) must be used as variable instead of scattering thickness, and scattering must compete with nuclear absorption (inelastic scattering) so that the gains are much more limited. The point is, of course, that *no* other means exist for performing equivalent operations. Further, the chromatic aberration may be used to bias a continuous energy spectrum to favor particular energies.

Our attention is directed primarily toward energies above a GeV. We will use neutrons for our numerical examples, although equivalent expressions almost certainly hold for K_0^L beams[3]). The expressions which play the role of eqs. (1)–(5) in the neutron case are given below, where the approximate analytic expressions are taken from the data of Parker et al.[4]) and Ringia et al.[5]) for 4–5 GeV neutrons. The elastic scattering is presumed here to be completely imaginary and due entirely to optical diffraction. In this case, then

$$\frac{d\sigma}{d|t|} = \frac{\sigma_T^2}{16\pi\hbar^2}\exp(-B|t|) = \frac{\sigma_T^2}{16\pi\hbar^2}\exp(-Bp^2\theta^2), \tag{22}$$

and since

$$\frac{d\sigma}{d\Omega} = \frac{p^2}{\pi}\frac{d\sigma}{d|t|},$$

$$\frac{d\sigma}{d\Omega} = \frac{p^2\sigma_T^2}{(4\pi\hbar)^2}\exp(-Bp^2\theta^2), \tag{23}$$

where p is in GeV/c. We will adopt the following approximate but very satisfactory dependences of σ_T and B on atomic number A:

$$\sigma_T = 80\, A^{\frac{2}{3}}\,\mathrm{mb} = 8\times 10^{-26}\, A^{\frac{2}{3}}\,\mathrm{cm}^2,$$
$$\tag{24}$$
$$B = 10\, A^{\frac{2}{3}}\,(\mathrm{GeV}/c)^{-2}.$$

If neutrons are incident on a slab of thickness l, the maximum number will emerge after experiencing a single scattering if the thickness is equal to the mean free path of neutrons in the material, i.e. $l = \lambda$, where

Fig. 7. The spectral enhancement of the "focussed" flux Φ in the focal plane of a scattering lens. The expression for $\Phi(p)/\Phi(p_0)$ is from eq. (18), with the assumption $\Phi_0(p) = \Phi_0(p_0)$.

$\lambda = A/(N\rho\sigma_T)$, with A the atomic number, N Avogadro's number, ρ the density, and σ_T the total cross section. The flux of single scattered neutrons Φ_s, is then given in terms of the incident flux, Φ_0, by

$$\Phi_s = \Phi_0 \frac{\sigma_{el}}{\sigma_T}\left(\frac{1}{e}\right), \qquad (25)$$

where σ_{el} is the elastic scattering cross section.

From eqs. (22)–(24),

$$\frac{\sigma_{el}}{\sigma_T} = \frac{\sigma_T}{16\pi\hbar^2 B} = 0.41, \qquad (26)$$

so that

$$\Phi_s/\Phi_0 = 0.1508.$$

As a result, if we neglect plural scattering, only 15% of the flux incident on a "lens" will be useful in scatter focussing.

We will explore four possible configurations of neutron lenses.

3.2. NEUTRON FOCUSSING WITH A A CONTINUOUS FUNCTION OF ANGLE

First, the exact analogue to the multiple Coulomb scattering case of section 2 may be studied, where the atomic mass number A replaces l as the continuous variable to maintain

$$\theta_{rms}\sqrt{2} = r/f.$$

We may repeat a measure of the treatment of section 2 by considering a coaxial scattering annulus of length λ in the z direction, average radius r and width dr, as in fig. 8. A flux Φ_0 in the $+z$ direction will result in an incremental flux $d\Phi$ at $+z = f$ from scattering in the ring given by

$$d\Phi = \Phi_0 \frac{2\pi r\,dr}{ef^2\sigma_T}\frac{d\sigma}{d\Omega}$$

$$= \Phi_0 \frac{2\pi p^2 \sigma_T}{(4\pi\hbar)^2 e}\theta\,d\theta\exp(-Bp^2\theta^2) \qquad (27)$$

$$= \Phi_0(3.76\times10^{25})p^2\sigma_T\theta\,d\theta\exp(-Bp^2\theta^2).$$

If we define $B^2 = 1/(2\theta_0^2)$ and use $\sigma_T/B = 8\times10^{-27}$ cm^2 (GeV/c)^2,

$$d\Phi = \Phi_0(0.3008)\times\frac{\theta\,d\theta}{2\theta_0^2}\exp-(\theta^2/2\theta_0^2). \qquad (28)$$

Now with A adjusted as a function of r so that

$\theta = \theta_0\sqrt{2}$, the integrated flux over a range of radii from r_1 to r_2 is given by

$$\Phi_s = \frac{0.3008}{e}\Phi_0\ln(\theta_2/\theta_1) = 0.1107\,\Phi_0\ln(\theta_2/\theta_1). \qquad (29)$$

This ratio Φ/Φ_0 is essentially the same Φ/Φ_0 as found in section 2, eq. (13) reduced by the factor 0.1508 of eq. (25). Unfortunately the range of θ_2/θ_1 is also constrained by available materials, since

$$\theta_0^2 \propto 1/B \propto A^{-\frac{2}{3}},$$

$$\theta_2/\theta_1 = (A_1/A_2)^{\frac{1}{3}}. \qquad (30)$$

A convenient span of materials would range from carbon to lead, where

$$(A_1/A_2)^{\frac{1}{3}} = (208/12)^{\frac{1}{3}} = 2.58.$$

One may do slightly better ranging from beryllium to uranium, with

$$(A_1/A_2)^{\frac{1}{3}} = (238/9)^{\frac{1}{3}} = 2.98$$

The overall enhancement factors are then

$$\Phi_s/\Phi_0 = 0.1049, \quad A \text{ from 12 to 208,}$$
$$\Phi_s/\Phi_0 = 0.1208, \quad A \text{ from 9 to 238.} \qquad (31)$$

In analogy with eqs. (13) and (19)

$$\Phi_T = \Phi_0[1 + 0.1107\ln(\theta_2/\theta_1)],$$

or

$$\Phi_T/\Phi_0 \cong 1.11. \qquad (32)$$

This is hardly a spectacular flux improvement.

It is however of greater interest here to consider the spectral response of such a lens. Neutron and neutral kaon beams from a multi-GeV accelerator are generally produced from a beryllium target in a proton beam. For zero degrees production the neutron spectrum is
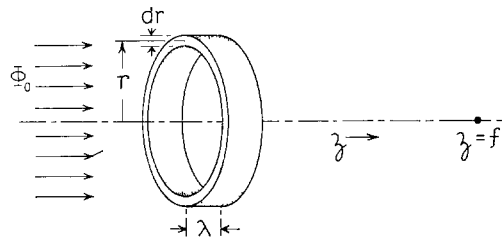
Fig. 8. Neutron scattering annulus of length $l = \lambda$ made of material with atomic number A.

roughly proportional to p^2 up to some momentum close to the proton momentum, beyond which the spectrum rolls off with a tail related to the Fermi motion of nucleons in the target nucleus[6]). The momentum spectrum enhancement provided by a diffraction-scattering lens would be exactly as represented in fig. 7, and by plugging the axis with several mean free paths of material, a neutron beam would be obtained of about 10% the original intensity and with a spectrum enhanced about a desired momentum. The undesirable aspect of such a lens, in addition to the intensity loss, is the angular divergence of the beam. In many experiments with high-energy neutrons the direction of an incident neutron is a necessary constraint in the data. This is normally quite well known from the event vertex and the neutron-producing target. In typical cases $p\theta$ is of the order of 1 to 0.3 MeV rad. With a carbon scatterer at θ_{rms}, $p\theta$ would be 140 MeV rad for a scatter-focussed beam.

It should be noted in both the flux and the spectrum calculations here and below that not only plural elastic scattering but all inelastic scattering has been ignored. It has been our experience in studying total cross sections and small angle elastic scattering of neutrons that the neglect of inelastically scattered neutrons over these small angles characteristic of the diffraction region is very appropriate. Charged particles and γ-rays are easily and effectively removed from such beams by sweeping magnets and radiators of high-Z materials.

3.3. THE HOMOGENEOUS PLATE NEUTRON LENS

We will now consider a different "lens" wherein a slab of a single material one interaction mean free path thick containing a small axial hole is used to enhance the neutron flux as in fig. 9. We will refer to this as the "homogeneous plate" case. In this case, eq. (28) may be integrated with θ_0 fixed to give

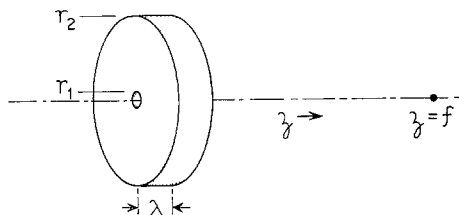$$\Phi_s = \Phi_0(0.150)[\exp(-\theta_1^2/2\theta_0^2) - \exp(-\theta_2^2/2\theta_0^2)]. \quad (33)$$

Fig. 9. Homogeneous plate neutron scatterer extending from r_1 to r_2 (subtending angles θ_1 and θ_2 from the focal point).

When $\theta^2_1 \ll \theta^2_0$, $\theta^2_2 \gg \theta^2_0$, this becomes simply

$$\Phi_s \cong 0.15\Phi_0,$$

and   (34)

$$\Phi_T = 1.15\Phi_0.$$

It seems at first surprising that this factor exceeds the factor 1.1 of eq. (32) for the "optimized" case. The reason, of course, is that the range of θ here is much greater. On the other hand, no spectral improvement is achieved here.

3.4. COMBINATION LENS

The third case which may be explored is one wherein a single, high-A medium is used from a minimum aperture to an intermediate radius, then a graded lens of the first type is used from this radius to the radius corresponding to θ_{rms} of the low-A medium, and the low-A medium then extended to a much larger radius. In this case the total gain in flux is indeed the sum of the two, i.e.

$$\Phi_T = \Phi_0(1+0.11+0.15) = 1.26\Phi_0. \quad (35)$$

Where maximum flux is the only criterion, this may be an interesting case. The total flux gain, however, seems relatively modest. Such a lens is illustrated diagrammatically in fig. 10.

3.5. A NEUTRON LENS OF THREE COAXIAL CYLINDERS

As a final case we may explore a simple and more realistic configuration in lieu of the lens of section 3.2 Nesting cylinders of three materials may be used, with one material of high atomic weight A_1 extending from r_a to r_b, a second of intermediate atomic weight A_2 from r_b to r_c, and a third light material of A_3 from r_c to r_d. Each cylinder would be an interaction mean free path in length, as illustrated in fig. 11. The ratios
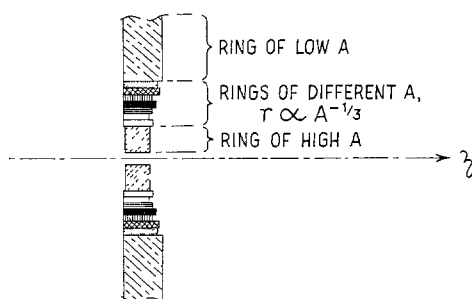

Fig. 10. Schematic section of combination lens with high atomic number medium inside and with low atomic number medium outside a region in which the atomic number is graded according to $r \propto A^{-1/3}$.

of the r's and A's may be chosen to yield the same terms in eq. (33) for each material. With angles θ proportional to radii r, we may define intermediate r.m.s. scattering angles θ_1, θ_2, and θ_3 as

$$2\theta_1^2 = (10\ A_1^{\frac{2}{3}} p^2)^{-1},$$

$$2\theta_2^2 = (10\ A_2^{\frac{2}{3}} p^2)^{-1},$$

$$2\theta_3^2 = (10\ A_3^{\frac{2}{3}} p^2)^{-1},$$

so that

$$A_1^{\frac{1}{3}}\theta_1 = A_2^{\frac{1}{3}}\theta_2 = A_3^{\frac{1}{3}}\theta_3.$$

We may set

$$\theta_b/\theta_a = \theta_c/\theta_b = \theta_d/\theta_c = \theta_1/\theta_2 = \theta_2/\theta_3,$$

and

$$\theta_b/\theta_a = (2^{\frac{1}{2}}\theta_1/\theta_a)^2, \text{ etc.}$$

This determines A_2 given A_1 and A_3 such that

$$A_2 = (A_1 A_3)^{\frac{1}{2}}. \tag{36}$$

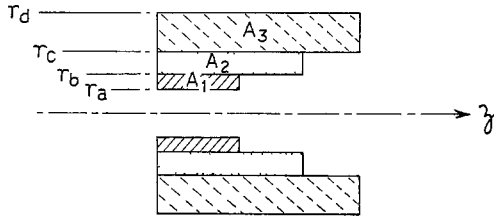The scattered flux Φ_s at the focal plane of the lens is

Fig. 11. Schematic section of three-element neutron lens of materials of atomic weights A_1, A_2 and A_3.
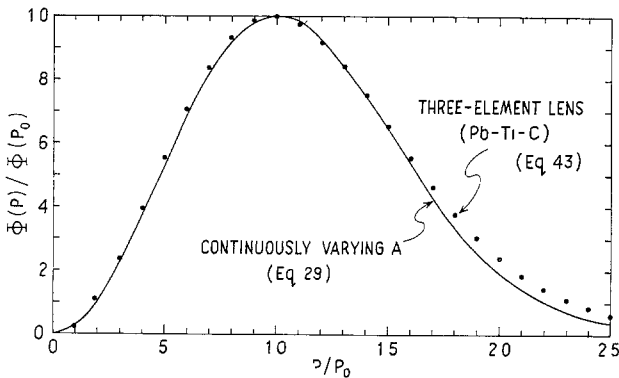

Fig. 12. The spectral response of a three-element neutron lens [eq. (43)], plotted as points, compared with the response of a continuously varying atomic number lens [eq. (29)]. The smooth curve is identically that of fig. 7, and again $\Phi_0(p) = \Phi_0(p_0)$ is assumed.

given in terms of the incident flux Φ_0 by

$$\Phi_s = \Phi_0(3 \times 0.15)[\exp(-\theta_a^2/2\theta_1^2) - \exp(-\theta_b^2/2\theta_1^2)], \tag{37}$$

and the spectral response will be

$$\Phi_s(p) = 0.45\Phi_0(p)[\exp(-p^2 B_1 \theta_a^2) - \exp(-p^2 B_1 \theta_b^2)]. \tag{38}$$

Two numerical examples are explored below. First, with $A_1 = 207.2$ (lead) and $A_3 = 12.01$ (carbon), $A_2 = 49.88$. Titanium, with $A = 47.90$ is suitably close. Second, with $A_1 = 238.1$ (uranium) and $A_3 = 9.02$ (beryllium), $A_2 = 46.34$, again close to 47.90 (titanium).

For the Pb–Ti–C lens,

$$(\theta_a/\theta_b) = (\theta_b/\theta_c) = (\theta_c/\theta_d) = 0.621. \tag{39}$$

From eq. (37),

$$\Phi_s = 0.45\Phi_0[e^{-0.621} - e^{-1.610}] = 0.152\Phi_0. \tag{40}$$

For the U–Ti–Be lens,

$$(\theta_a/\theta_b) = 0.5794, \text{ etc.} \tag{41}$$

and

$$\Phi_s = 0.172\Phi_0. \tag{42}$$

From eq. (38), the spectra in the two cases are given by, first,

$$\Phi_s(p)/\Phi_s(p_0) = \frac{1}{0.33752} \times$$
$$\times \{\exp[-0.621(p/p_0)^2] - \exp[-1.61(p/p_0)^2]\}, \tag{43}$$

and, in the second case,

$$\Phi(p)/\Phi(p_0) = \frac{1}{0.38224} \times$$
$$\times \{\exp[-0.5794(p/p_0)^2] - \exp[-1.726(p/p_0)^2]\}. \tag{44}$$

This spectral response is graphed in fig. 12 together with the spectral response of eq. (29) of section 3.2 (fig. 7). The shape of the response is remarkably similar to that from the structurally impractical continuum of materials.

It may be interesting to consider a numerical example relevant to the new NAL accelerator. Consider a lens optimized for 300 GeV neutrons, with the relationship from eqs. (27) and (24), e.g.

$$1/\theta_a = f/r_a = 10^{\frac{1}{2}} p_0 A_1^{\frac{1}{3}}(\theta_b/\theta_a)^{\frac{1}{2}}, \text{ etc.}$$

The parameters for a lens of focal length $f = 100$ m are noted in table 1.
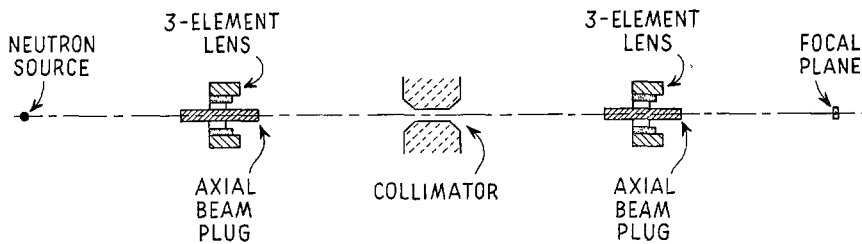
Fig. 13. Schematic section of two-stage neutron beam employing two three-element lenses containing axial beam plugs and a collimator at the first focus.

TABLE 1

Lenses of 100 m focal length optimized for $p_0 = 300$ GeV/c neutrons.

Material	Length (cm)	Radius (cm)	Φ_s/Φ_0
Pb	9.5	1.404	
Ti	16.8	2.260	0.152
C	23.8	3.639	
		5.858	
U	6.9	1.294	
Ti	16.8	2.234	0.172
Be	24.0	3.856	
		6 655	

At NAL there is a neutron beam brought to detectors about 400 m from the neutron production target. By locating such a lens at 200 m from the target and plugging the central hole with an iron rod absorber of at least 1 m, and placing a collimator of 1 or 2 cm aperture at 400 m, an enriched flux of about 15% of the original beam (through that aperture) would be achieved.

3.6. TWO-STAGE NEUTRON FOCUSSING

It was suggested by Gustafson that in some cases the neutron flux is much greater than needed and that the shape of the spectrum is all important, so that it might be desirable to use a second lens in tandem with the first. The flux at the focus of the second lens would now be about 15% of the *flux* incident on the second lens, if it were incident as a parallel beam. In fact, the flux is diverging from the first focus, so that if the second lens is half way between the first and the second foci, the final flux is reduced an additional factor of four. The situation is sketched in fig. 13. The *number* of neutrons at the second focus, N_2, is given by

$$N_2 = \Phi_2 A_2 = \frac{0.152}{4} \Phi_0' A_2,$$

where Φ_0' is the flux incident on the second lens. If N_1 is the number of neutrons transmitted through the first collimator, A_1 is the area of the first collimator, and A_L the area of the lens,

$$N_1 = \Phi_s A_1 = \Phi_0' A_L,$$

so that

$$N_2 = \frac{0.152}{4} \Phi_s \frac{A_1 A_2}{A_L} = \frac{(0.152)^2}{4} \Phi_0 \frac{A_1 A_2}{A_L},$$

or

$$\Phi_2 = (5.8 \times 10^{-3} \, A_1/A_L)\Phi_0.$$

For a 2 cm diameter aperture A_1 and the Pb–Ti–C lens of table 1,

$$\Phi_2 = 1.79 \times 10^{-4} \, \Phi_0.$$

This assumes both lenses contain plugs to block the axial beam, and applies only to the "design" momentum p_0.

The resulting spectral response, which is achieved at the cost of this loss, is the square of the curve of fig. 12 and is plotted in fig. 14. It appears to us that
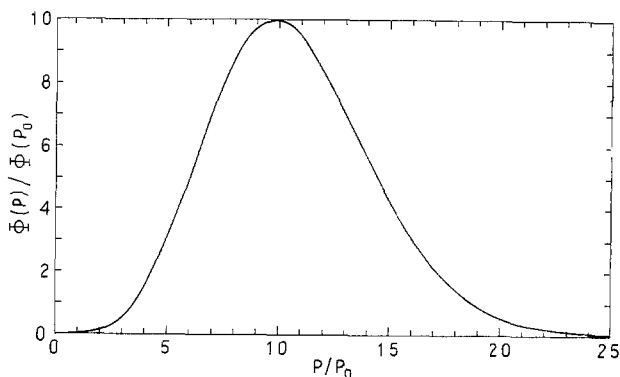

Fig. 14. The spectral response of the two-stage, three-element lens system of fig. 13. The ordinate values are the squares of the corresponding values of fig. 12.

only rarely will such a loss in flux justify the spectral response gain.

4. Conclusions

We have shown how very simple multiple scattering lenses may provide flux enhancements of charged particles by modest factors ($\times 2 - \times 4$). The practical utilization of such lenses may be very limited except for such special applications as neutrino beams.

Multiple Coulomb scattering also provides the basis for a curious form of radiography using multi-GeV charged particles. Here discontinuities in scattering properties are visualized yielding results somewhat analogous to Xerographic X-rays.

Utilizing similar mathematics, the nuclear elastic scattering of multi-GeV neutrons and other neutral hadrons serves as a mechanism for focussing such particles. The absolute flux gain thus achieved in neutral hadron beams is less than 50%, however the chromatic aberation of such lenses may serve to provide a differential flux enhancement such that a spectrum may be peaked about a desired momentum.

A two-stage lens system is possible, although the greater spectral improvement is only achieved with severe loss of flux.

The authors have profited from ideas and conversations with our colleagues in the University of Michigan high-energy groups. We would like to thank particularly Prof. T. Bowen of the University of Arizona for pointing out an error in the earlier treatment of ref. 1, and Prof. M. L. Perl of S.L.A.C. for his assistance in the Cosmotron experiments.

References

[1] L. W. Jones, *The random optics of particle beams* (Univ. of Michigan Technical Report 03106-15-T, 1964) unpublished. L. W. Jones, 12th Intern. Conf. High Energy Physics, vol. 2 (Atomizdat, Moscow, 1966) p. 569.

[2] B. Rossi, *High energy particles* (Prentice Hall, 1952) p. 66. W. H. Barkas and A. H. Rosenfeld, UCRL-8030 TID-4500 (1963) unpublished.

[3] W. L. Lakin, E. B. Hughes, L. H. O'Neill, J. N. Otis and L. Madansky, Phys. Lett. **31B** (1970) 677.

[4] E. F. Parker, T. Dobrowolski, H. R. Gustafson, L. W. Jones, M. J. Longo, F. E. Ringia and B. Cork, Phys. Lett. **31B** (1970) 246.

[5] F. E. Ringia, T. Dobrowolski, H. R. Gustafson, L. W. Jones, M. J. Longo, E. F. Parker and B. Cork, Phys. Rev. Lett. **28** (1972) 185.

[6] B. G. Gibbard, Thesis (Report UM-HE-70-11, Randall Laboratory of Physics, University of Michigan, 1970) unpublished. T. P. McCorriston, Jr., Thesis (Report UM-HE-72-11, Randall Laboratory of Physics, University of Michigan, 1972) unpublished. D. D. O'Brien, Thesis (Report UM-HE-72-32, Randall Laboratory of Physics, University of Michigan, 1972) unpublished.